journal

J. Am. Ceram. Soc., 98 [7] 2278–2285 (2015)
DOI: 10.1111/jace.13559

Raman and X-ray Studies of Uranium–Lanthanum-Mixed Oxides Before and After Air Oxidation

Zeynep Talip,† Thierry Wiss, Philippe E. Raison, Jérôme Paillier, Dario Manara, Joseph Somers, and Rudy J.M. Konings

European Commission, Joint Research Centre, Institute for Transuranium Elements, P. O. Box 2340, Karlsruhe 76125, Germany

UO_2 samples doped with 6, 11, 22 mol% lanthanum were examined before and after air oxidation. To verify the formation of uranium–lanthanum-mixed oxide solid solutions, powder X-ray diffraction (XRD) analyses of the crystalline phases in the materials were carried out. The presence of oxygen vacancies in the La-doped UO_2 samples was identified by Raman spectrometry. It was evidenced by changes induced in the Raman spectra by air oxidation. This latter was carried out either by increasing the Raman laser power or by thermally treating the samples at 500 K for 370 h. In addition, oxidation behavior differences of pure and La-doped UO_2 samples were reported by comparing XRD and Raman results of the samples before and after air oxidation. It was shown that the concentration of the M_4O_9 (M: U, La) phase increased with increasing content of La, whereas inhibition for the formation of M_3O_8 phase was observed.

I. Introduction

The lanthanide elements have high fission yields and are known to form solid solutions with UO_2 over a wide range of compositions. As the yield of fission product lanthanum in the fission of uranium is relatively high, uranium–lanthanum-mixed oxides have been studied by various authors.[1–9] Lanthanum is dissolved in UO_2 to form a solid solution (U, La)$O_{2\pm x}$ with a fluorite structure, where the La^{3+} ions substitute on the uranium sublattice and can create an oxygen vacancy environment that is similar to the hypostoichiometric UO_{2-x}. The crystal chemistry of this solid solution, could be described as $(U^{4+}_{(1-x-y)},U^{5+}_{(x)},La^{3+}_{(y)})(O_{(2+x/2-y/2)})$ with the special cases $(U_{1-y}^{4+},La_y^{3+})O_{(2-y/2)}$ ($[U^{5+}] = 0$) and $(U^{4+},U^{5+},La^{3+})O_2$ ($[U^{5+}] = [La^{3+}]$) and $(U^{4+},U^{5+},La^{3+})O_{2+x}$ ($[U^{5+}] > [La^{3+}]$).

Nevertheless, the effect of lanthanides dopants on the oxidation of UO_2 still presents open question calling for further research.[10–14] It is known that there are significant differences in air oxidation behavior between unirradiated and spent UO_2 fuel.[15] Choi *et al.*[13] suggested that dissolved fission products can modify the oxidation kinetics of the spent fuel. It was shown that UO_2 with lanthanide dopants increases the stability of the cubic fluorite structure (compared to that of undoped UO_2) with respect to U_3O_8.[13]

In this study, XRD and Raman techniques were used to characterize the pure and three different uranium–lanthanum-mixed oxides. The paper is divided into two parts. The first part describes the La-doping effect on the UO_2 structure. The second part describes the low-temperature air oxidation effect on pure and La-doped UO_2 samples.

II. Experimental Procedure

(1) Samples

La-doped UO_2 samples with three different compositions (6, 11, 22 mol%) were prepared by a sol–gel technique.[16] Transmission electron microscopy observations on several grains of La-doped UO_2 samples showed that all the samples have homogeneous compositions and no La or U oxide precipitates were present in the samples.[17] The obtained powders were pressed at 110 MPa into a disk and the compacted disks were sintered at 1923 K for 6 h under 6% H_2/94% Ar atmosphere to have $(U_{1-y}^{4+},La_y^{3+})O_{2-y/2}$, that is, containing only U^{4+},[18] and the O/M ratios of the three samples are thus O/M = 1.97, 1.945, ad 1.89, respectively. After sintering, the samples thickness was ~0.4 mm. The uranium and lanthanum concentrations of the samples were determined by energy dispersion X-ray spectroscopy, EDS (Oxford detector mounted in a Vega Tescan TS5130LSH operated at 30 KeV, Brno, Czech Republic).

Undoped UO_2 samples used are commercial UO_2 pellets (Siemens AG) with an average grain size of about 14 μm. The pellets were cut and drilled to obtain disks (3 mm diameter and 0.4 mm thickness) similar to the La-doped samples. The samples were then annealed in an alumina furnace for 10 h at 1500 K under a constant gas flow of Ar 94%/H_2 6% to recover surface defects and to restore the stoichiometry of the samples.

U_4O_9 powder was used as a reference material for Raman analyses. The U_4O_9 sample was prepared by heat-treatment of a mixture of UO_2 and U_3O_8 powder.[19] UO_2 and U_3O_8 powders were put in a quartz tube where primary vacuum (3.7×10^{-3} mbar) was made before sealing. It was heated at 1373 K (heating and cooling rate: 573 K/h) for 1 month. Different batches were prepared and the best quality U_4O_9 sample was chosen by XRD analyses and used for Raman measurement.

Subsequently, air oxidation of the pure and La-doped UO_2 samples were performed at 500 K for 370 h.

(2) XRD Measurements

Powder X-ray diffraction analyses were performed to analyze the phase and lattice parameter of the samples with a Bruker (Billerica, MA) D8 X-ray diffractometer mounted in a Bragg–Brentano configuration, with a curved Ge monochromator (111), a ceramic Cu X-ray tube (40 kV, 40 mA) and a Linxeye detector covering 3° in 2θ. Scans were collected from 20° to 120° in 2θ using 0.0086° step intervals with counting steps of 5 s. The lattice parameters of the samples were obtained from Rietveld refinement (using the Fullprof program)[20–22] applied to the $Fm\bar{3}m$ space group.

T. Besmann—contributing editor

Manuscript No. 35734. Received October 5, 2014; approved February 20, 2015.
†Author to whom correspondence should be addressed. e-mail: zeynep.talip@gmail.com

(3) Raman Spectroscopy Measurements

Raman spectra were measured with a Jobin–Yvon® T64000 spectrometer (Kyto, Japan) used in the single spectrograph configuration. The excitation source was a Kr^+ (Santa Clara, CA) Coherent®continuous wave laser radiating at 647 nm having a tunable nominal power ranging from 10 to 750 mW at the exit of the cavity. The power impinging the sample surface (lower approximately by a factor of 10) was measured by a calorimeter. Spectra are measured in a confocal microscope with a 50-fold magnification and long focal distance. This feature allows obtaining a good spectral resolution (± 1 cm^{-1}) independently of the surface shape, with a spatial resolution of 2 μm × 2 μm on the sample surface. The spectrograph angle is calibrated with the T_{2g} excitation of a silicon single crystal, set at 520.5 cm^{-1}.[23] The spectral data were acquired with an exposure time of 180 s and accumulations over the wave number range from 200 to 1300 cm^{-1}. It was experimentally found that a 2 mW laser power at the sample surface has no detectable oxidation effects on the initial material surface if the exposure time does not exceed 180 ms. Such power level was therefore adopted in all the current Raman measurements. The 488 nm line of an Ar^+ Coherent laser was also used as an excitation source for comparison, with a nominal power varying between 1 and 20 mW.

III. Results and Discussion

(1) UO_2 and La-Doped UO_2 Samples

(A) X-ray Diffraction: The solid solution between lanthanum oxide and uranium dioxide exists in a large range of compositions. The solubility limits of La were reported as 0–54 mol% at 2013 K, under vacuum,[10] 0%–75% at 2023 K,[1] 0%–82% at 1523 K, 25%–82% at 1823 K, under reducing conditions[3,7] and 0%–67% at in oxidizing atmosphere.[3,7] In this study, the XRD results showed that the La-doped UO_2 samples were single-phase solid solutions with a fluorite type structure for the full doping range (6, 11, 22 mol%) studied (Fig 1).

The defect structure of La-doped UO_2 has been previously studied by different authors.[5,24,25] Matsui *et al.*[5] studied the oxygen partial pressure influence on electrical conductivity and deviation from stoichiometry for La-doped UO_2 samples. They proposed a complex defect model for $(U_{1-y}La_y)O_{2\pm x}$ with oxygen vacancies and interstitial oxygens. Desai also suggested two charge compensation mechanisms for La^{3+} in UO_2 based on Mott–Littleton simulations.[24] Her calculations showed that in the case La is introduced into uranium dioxide, the lattice expansion is much larger if the charges are compensated by oxygen vacancies instead of U^{5+}. Obviously, these oxygen vacancies have a strong affinity for oxygen and are easily filled by oxygen atoms in an oxidizing atmosphere.[26] Shin and Besmann[25] also considered both mechanisms (oxygen vacancy and U^{5+} formation compensation) in the sublattice model used to describe the thermodynamic properties (oxygen potentials) of the $(U,La)O_{2\pm x}$ phase. The types of solid solution formed $[(U,La)O_{2+x}$ or $(U,La)O_{2-x}]$ are stable in both reduced and oxidized conditions. The stoichiometry variance of La-doped UO_2 samples depends on La concentration and oxidation state of the uranium which is related to the oxygen potential present during sample preparation.[1] However, the precise determination of the oxygen-to-metal (O/M) ratio for lanthanide-doped uranium dioxides is technically quite difficult. Krishnan *et al.*,[27] performed X-ray photoelectron spectroscopy studies on uranium–lanthanum-mixed oxides. They observed that the surface O/M ratios are greater than two in U-rich mixed oxides and less than two in La-rich mixed oxides, whereas the bulk O/M in all the samples are less than two. In this study, La-doped UO_2 samples were U-rich and prepared under reducing conditions, for which we assume that the uranium is in a 4+ state only. For these samples, the first mechanism (oxygen vacancy formation) is more relevant. It is known that the dissolution of trivalent lanthanide oxides in UO_2 results in a negative shift in the lattice parameter except for $LaO_{1.5}$.[7,26,28,29] The ionic radius of La^{3+} (0.1160 nm) is much larger than that of U^{4+} (0.1001 nm). Although the oxidation of U^{4+} results in a decrease in the lattice parameter, its contribution is less than the increase due to doping with La ions.[8,30] The variation in the lattice parameter of $(U_{1-y}La_y)O_{2-y/2}$ with the concentration of lanthanum is shown in Fig 2. The lattice parameter increases linearly with the increase in the lanthanum concentration and with the linear correlation $a = 5.4712 + 0.0007\ [y]$ [a being the lattice parameter (Å), y La content %].

(B) Raman Spectroscopy: Raman spectroscopy is sensitive to defects of the O sublattice in UO_2. This allows us to perform a qualitative characterization of hypostoichiometry in La-doped UO_2 samples. According to our knowledge there is no available reference data on Raman spectrum of La-doped UO_2 materials.

Raman spectra of the undoped UO_2 sample were acquired in a first step (Fig. 3) and the main bands observed were compared with published data.

Five specific spectral features can be identified in the pure UO_2 Raman spectrum displayed in Fig. 3.

For band (1), group theory predicts that UO_2 has one triply degenerate Raman active mode (T_{2g}),[31,32] characteristic of the stoichiometric fluorite structure, appearing here at 445 cm^{-1}, in agreement with existing literature data.[32–36] The same Raman band was observed at 448 cm^{-1} for UO_2 single crystal and 446 cm^{-1} for UO_2 polycrystalline by Graves *et al.*[31]

Bands (2) and (5) centered at 575 and 1150 cm^{-1} were recently assigned, respectively, to 1 longitudinal optical (LO)

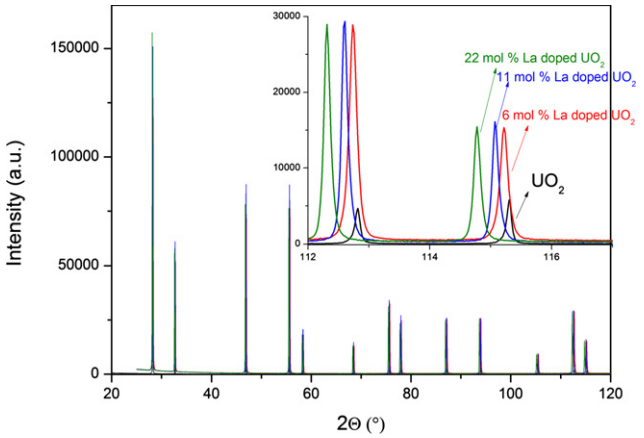

Fig. 1. X-ray diffraction pattern of UO_2 and La-doped UO_2 samples, a comparison of the Bragg reflection profile in the 110–120 2θ reflections from all the samples studied is shown in the inset.

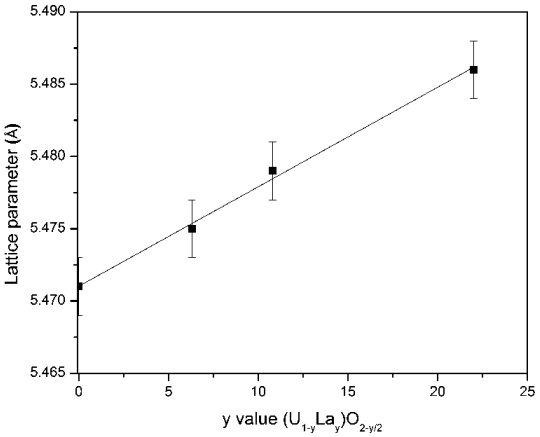

Fig. 2. Lattice constants from pure UO_2 to $(U_{1-y}La_y)O_{2-y/2}$ samples as measured by XRD.

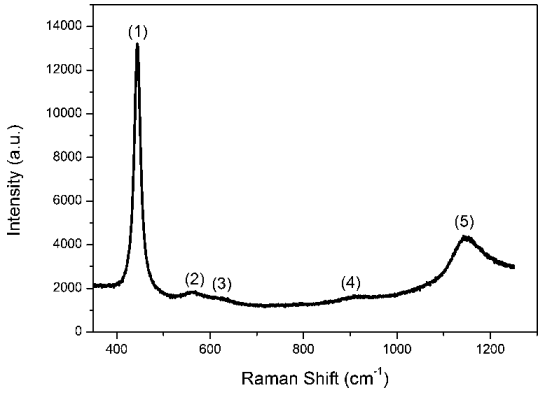

Fig. 3. Raman spectra of UO_2 (conditions: 647 nm, excitation: 2 mW, exposure time: 180 s, 350–1300 cm^{-1}).

and 2 LO phonons by Livneh and Sterer.[37] These authors soundly proved, with the help of energy- and pressure-dependent Raman scattering, that the broader band located at 1150 cm^{-1} is a Raman resonant overtone of the LO phonon band intersecting the Γ limit of the Brillouin zone at 575 cm^{-1}. Manara *et al.*[37] showed that the 2LO band can be regarded as a fingerprint of a quasiperfect fluorite structure in UO_2.

According to Desgranges *et al.*,[39] band (3) observed at about 630 cm^{-1} can be assigned to a Raman mode activated by the presence of structural defects in the cub octahedral symmetry of the interstitial oxygens in hyperstoichiometric UO_2. A regular distribution of such interstitial oxygen atoms leads to the formation of U_4O_9 crystallites. Therefore, the Raman mode at 630 cm^{-1} can be regarded as a sign of the presence of a defective U_4O_9 structure.

The broad band around 800–900 cm^{-1} (4) was attributed to the presence of uranyl ion-containing phases, which could be due to a slight air oxidation of the sintered UO_2 surface.[40]

Figure 4 shows the Raman spectra of La-doped UO_2 samples over the wave number range from 200 to 1300 cm^{-1}. Measurements were repeated at different points on the surface of each sample to confirm that the recorded spectra were representative of the whole sample. A loss of relative intensity in the T_{2g} band would indicate deviations from the perfect cubic fluorite structure, consistent with the formation of oxygen vacancies in the lattice.[41]

The characteristic 1150 cm^{-1} 2LO band of UO_2 was observed only for $(U_{0.94}La_{0.06})O_{1.97}$ sample (Fig. 4) and it disappeared when increasing the La content of the sample. Similar behavior was observed for hyperstoichiometric UO_2 samples.[38,42] The intensity of 2LO band decreased by increasing oxygen content of the sample and was not observed for highly oxidized UO_2 samples. In addition, the resonance Raman effect is often observed when the laser excitation energy is comparable to the band gap energy.[43] Taniguchi *et al.*[44] reported that when band-gap energy of pure and Gd^{3+}-doped CeO_2 materials matched the excitation energy, the second-order Raman bands' intensity dramatically increased.

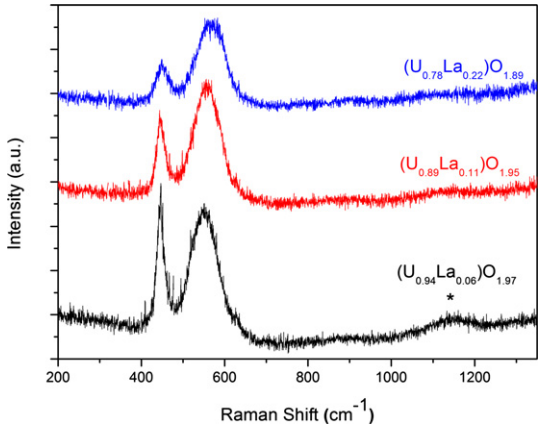

Fig. 4. Raman spectra of $(U_{0.94}La_{0.06})O_{1.97}$ (black line), $(U_{0.89}La_{0.11})O_{1.95}$ (red line), and $(U_{0.78}La_{0.22})O_{1.89}$ (blue line) samples (conditions: 647 nm, excitation: 2 mW, exposure time:180 s, 200–1300 cm^{-1}).

A broad band at ~550–570 cm^{-1} was observed for all the La-doped UO_2 samples (Fig. 4). It slightly shifts to the higher wave numbers with increase in the La content in the sample. Defect structure of UO_2 was studied with Raman spectroscopy by He *et al.* and the broad band between 500 and 700 cm^{-1} was attributed to UO_2 lattice damage due to the presence of lattice defects.[42]

Deconvolution of this broad band into three bands for all the La-doped UO_2 samples were shown in Figs. 5(a)–(c). A band at 540 cm^{-1} was observed for all the samples. Recently Razdan and Shoesmith[45] studied the trivalent dopant influence on the UO_2 structure and a strong Raman band at 540 cm^{-1} was attributed to the O vacancies in SIMFUEL, Gd-doped UO_2, and Dy-doped UO_2 samples. This feature was previously shown by similar studies performed on cerium dioxide,[46–48] which has the same crystal structure and many similar material properties as uranium dioxide and is therefore used as a good surrogate material for uranium dioxide in literature.[49–52] For example, McBride *et al.*[46] studied $Ce_{1-x}RE_xO_{2-y}$ samples by Raman spectroscopy and they observed a broad band near 570 cm^{-1} which was attributed to O vacancies. They could also obtain similar results considering oxygen vacancies effect in CeO_2 system with Grenn's function model calculations. Guimbretiere[53] and Desgranges[54] also observed a band around 530 cm^{-1} for He^{2+} implanted UO_2 samples. It has been pointed out that this band could be the Raman signature of defects in UO_{2-x} resulting from implantation. Desgranges[55] proposed the formation of new types of defect (Magnéli type defects) for He^{2+}-implanted UO_2 samples. Magnéli type defects generate an area with U^{3+} or U^{5+} in which formation of the oxygen sublattice defects would be possible. This is a similar defect structure as the one formed in M^{3+}-doped UO_2 samples. Raman results of (U, Nd)O_{2-x} samples also showed a band at 530 cm^{-1} which was interpreted as a local phonon mode associated with oxygen-vacancy-induced lattice distortion.[56] Moreover, this band is not observed in Th-doped UO_2 samples. As 4+ oxidation state of thorium is stable, it is not surprising that oxygen vacancy clusters are not formed in the system which also confirms the assignment of this band.[57] In this study, it was also observed that the relative intensity of the 540 cm^{-1} band to T_{2g} band, systematically increased with increasing La^{3+} content of the samples, consistent with the increasing oxygen vacancy concentration in the samples with La content [Fig. 5(d)].

The band at 575 cm^{-1} has been attributed to longitudinal optical (LO) T1u vibration mode which is visible in Raman due to the crystal lattice disorders.[37] Graves,[31] Guimbretiere *et al.*[53] and Desgranges *et al.*,[54] observed a similar at ~575 cm^{-1}, attributed to lattice damage resulting from the Kr and He^{2+} implantation for UO_2 samples, respectively, and they have reported that the intensity of this band increased with increasing radiation damage of the sample.

Asymmetric tailing of this broad band toward higher wave numbers was observed with only a very small contribution for all the La-doped samples [Figs. 5(a)–(c)]. This high-energy tail may be associated with the formation of higher oxides due to the sample surface oxidation during handling. As mentioned above, the band at 630 cm^{-1} was recently attributed to the presence of defective U_4O_9 (clusters of interstitial oxygen atoms) by Desgranges *et al.*[39]

Hence, in this study the Raman spectrum of U_4O_9 was measured under the same conditions (Fig. 6) to help the interpretation of this band in La-doped UO_2 samples. Splitting of the bands and numerous minor bands of various

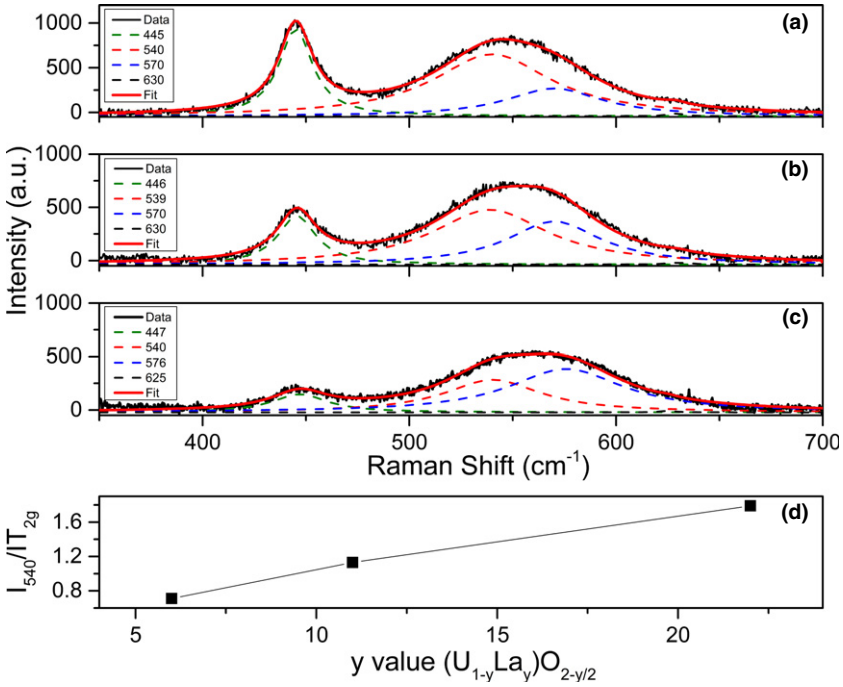

Fig. 5. Raman spectra recorded on $(U_{0.94}La_{0.06})O_{1.97}$ (a), $(U_{0.89}La_{0.11})O_{1.95}$ (b) and $(U_{0.78}La_{0.22})O_{1.89}$ (c) samples and deconvolutions of contiguous bands at ~445, 540 and 570 cm^{-1} (deconvolution with Lorentzian peak model), plot of I_{540}/I_{T2g} with a y value of $(U_{1-y}La_y)O_{2-y/2}$ (d).

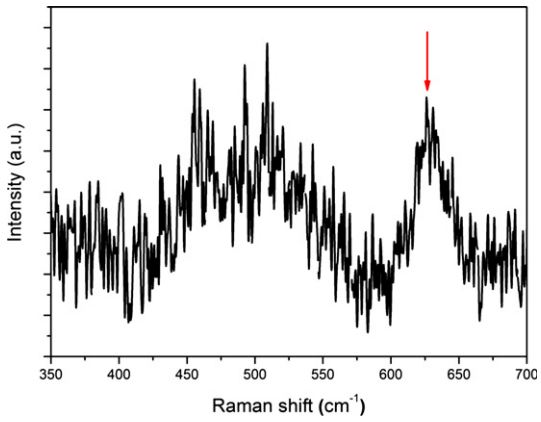

Fig. 6. Raman spectrum of a U_4O_9 sample (conditions: 647 nm, excitation: 2 mW, exposure time:180 s).

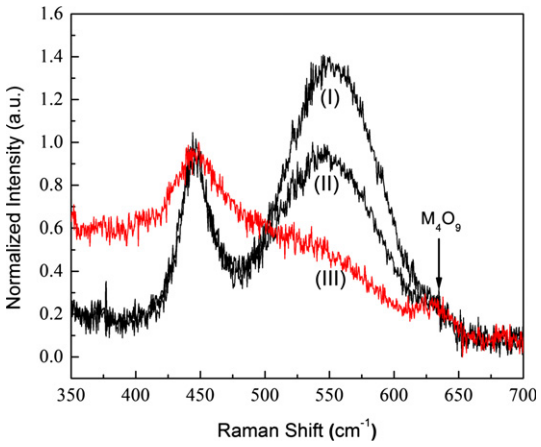

Fig. 7. Raman spectra of $(U_{0.89}La_{0.11})O_{1.95}$ sample under (I) 2 mW, (II) 6 mW, (III) 13 mW (conditions: 647 nm, exposure time:180 s).

positions and intensities between 400 and 600 cm^{-1} were observed. This was attributed to the existence of trace amount of U_3O_8 which was also shown by its XRD pattern in the prepared U_4O_9 powder. However, only a sharp and well defined band is located at ~630 cm^{-1} as it was previously reported by Desgranges *et al.*[39] Therefore, one can conclude that the similar band that is systematically observed especially for oxidized La-doped UO_2 samples (see the following section) should be attributed to the formation of a M_4O_9 structure also in these compounds.

A further test was performed in the current research to check for effects of the potential sample surface oxidation occurring during the Raman measurements due to the heating effect of the laser beam. It is known that solid solutions containing oxygen vacancies are sensitive to oxidation.[26] Oxidation of the sample by increasing laser power as a heat source was reported by Palacious[58] on UO_2 and Jégou[59] on UO_2 and $(U_{1-y}Pu_y)O_2$ samples. Oxidation of the samples under Kr^+ laser beam was shown by recording the spectra sequentially on the same point of the sample at the consecutive laser powers (I) 2, (II) 6, and (III) 13 mW (at the exit of the laser cavity). Figure 7 shows the oxidation of the 11 mol % La-doped UO_2 samples by the laser beam. As can be seen, the laser beam heated the sample which has an effect, although not quantified, on the measured Raman spectrum. By increasing the laser power the intensity of the second band, also attributed to oxygen vacancies, decreases due to oxidation. The same tendency was also observed for 6 and 22 mol% La-doped UO_2 samples. The presence of the 630 cm^{-1} band is more clearly revealed. This observation confirms the attribution of the 540 cm^{-1} Raman mode to the presence of oxygen vacancies, and the 630 cm^{-1} band to the formation of M_4O_9.

Raman measurements were also performed on pure UO_2, La-doped UO_2 and U_3O_8 samples with a 488 nm Ar^+ ion laser. The Raman bands of U_3O_8 were previously reported at 236, 342, 408, 480, 752, 798, and 888 cm^{-1} by Allen[34] and Butler.[60] By comparing the Raman spectra of pure U_3O_8 and UO_2 samples (Fig. 8) it was found that the pure UO_2 sample was oxidized during the measurement to U_3O_8 due to the localized heating of the sample with high laser power. Figure 8 also shows the Raman spectra of the La-doped

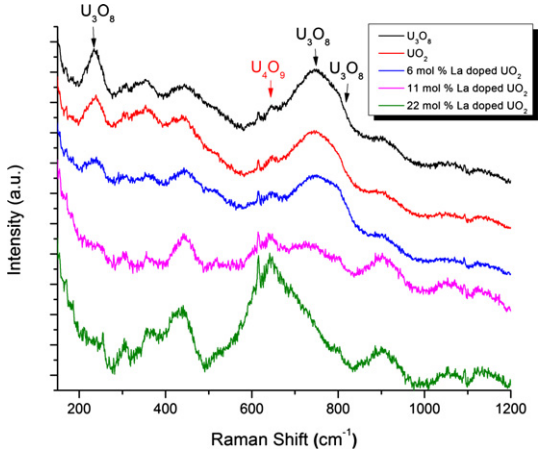

Fig. 8. Raman spectra of U_3O_8, UO_2, $(U_{0.94}La_{0.06})O_{1.97}$, $(U_{0.89}La_{0.11})O_{1.95}$, and $(U_{0.78}La_{0.22})O_{1.89}$ samples (conditions: Ar^+ laser at 488 nm, excitation: 10 mW, exposure time: 180 s).

UO_2 samples recorded under these conditions. The broad band around 900 cm^{-1}, which was attributed to uranyl-containing phases,[40] was observed for all the samples. Comparison of the Raman spectra shows the inhibition of the formation of U_3O_8 phase with increasing La content, especially for 22 mol% La-doped UO_2 sample as the intensities of the strong Raman bands at 236, 752, and 798 cm^{-1} were decreased and the intensity of M_4O_9 band increased.

(2) Low-Temperature Air-Oxidized UO_2 and La-Doped UO_2 Samples

X-ray Diffraction: To shed more light on the air oxidation of La-doped UO_2 samples, this process have studied more systematically in this research. Air oxidation of pure and La-doped UO_2 samples was performed at 500 K for 370 h. Oxidation of UO_2 doped with impurities proceeds via $UO_2 \rightarrow U_4O_{9+y} \rightarrow U_3O_8$. The idea was to study first stage of oxidation. Therefore, 500 K was chosen for the oxidation test, as the rate of U_3O_8 formation is extremely slow below 500 K.[61] XRD analyses showed that after air oxidation, the pure UO_2 samples were a single phase with no significant changes in the X-ray diffraction data, whereas all La-doped UO_2 samples were constituted of two phases (MO_{2+x} and M_4O_9). However, further reaction to M_3O_8 was not observed for any of the samples. This can be clearly seen in the XRD patterns in the 2θ range from 100° to 120° that are shown in Fig. 9. Consistently, the weight gain measured in oxidized La-doped UO_2 samples were much higher than in undoped UO_2. This behavior could be due to the more rapid oxygen diffusion in La-doped samples. Kim and Olander[62] reported that oxygen diffusion in UO_{2-x} is much faster than in UO_2, consistently with the anion vacancy as the primary defect in UO_{2-x}. La doping causes a lattice expansion in UO_2 which could also increase diffusion of O^{2-} ions in doped UO_2 matrix. Furthermore, although oxidation of pure and La-doped UO_2 samples was performed under the same conditions (sample thickness, oxidation temperature, and time), oxidation of UO_2 could also depend on other parameters such as grain size, density, and orientation effect.[61] The grain size of the current La-doped UO_2 samples was in fact much smaller compared to undoped UO_2 (The average grain sizes of 6, 11, 22 at.% La-doped UO_2 and undoped UO_2 samples are 3, 4, 7, and 14 μm, respectively.[17] This would also explain a more rapid oxygen diffusion along grain boundaries than into the larger UO_2 grains.[61]

Thomas *et al.*[15] showed that the presence of lanthanides in unirradiated UO_2 stabilizes the cubic M_4O_9 crystal lattice during air oxidation at low temperature (175°C–195°C) and delays the formation of M_3O_8 similar to the oxidation behavior of Light Water Reactor spent fuel. The phase contributions for the air-oxidized samples were obtained from Rietveld refinement and the results presented herein show clearly that an increase La content in UO_2 results in higher M_4O_9 (M = U, La) phase contribution (Fig. 9, Table I). It shows that increasing La increases the first stage oxidation kinetics $[U_xLa_yO_{2-y/2}$ to $(U_xLa_y)_4O_9]$. Ha *et al.*[63] oxidized the thorium-doped UO_2 samples and they observed that the first step of the oxidation kinetic curves show the same gradient for all the $(U_{1-y}Th_y)O_2$ samples(y: 0–0.27). In contrast, it was reported by Kim *et al.*[64] that Gd dopant slows down the reaction from $(U_{1-y}Gd_y)O_2$ to $(U_{1-y}Gd_y)_4O_9$. These results could be explained by the influence of doping on the fluorite lattice parameter. In the case of doping UO_2 with La or Th leads to an increase in lattice parameter, whereas Gd doping causes a decrease. The expansion of the fluorite lattice increases the oxygen mobility

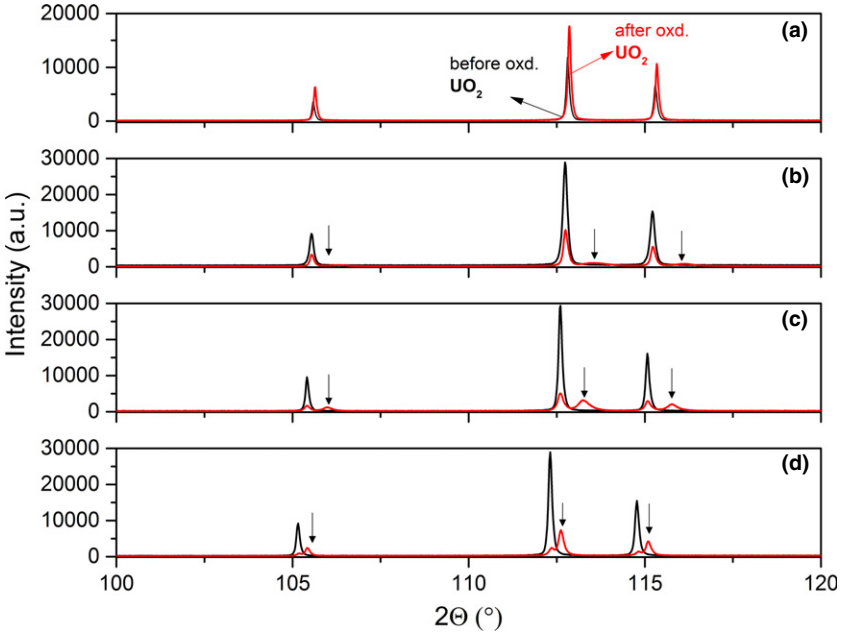

Fig. 9. Bragg reflection profile in the 100–120 2θ reflections from X-ray diffraction patterns of UO_2 sample (a), $(U_{0.94}La_{0.06})O_{1.97}$ (b), $(U_{0.89}La_{0.11})O_{1.95}$ (c), and $(U_{0.78}La_{0.22})O_{1.89}$ (d) before (black line) and after air oxidation (red line).

Table I. Lattice Parameters and Phase Contributions of the La-Doped UO_2 Samples After Air Oxidation (500 K 370 h)

	6 mol% La-doped UO_2		11 mol% La-doped UO_2		22 mol% La-doped UO_2	
	MO_2	M_4O_9	MO_2	M_4O_9	MO_2	M_4O_9
Lattice parameter (Å)	5.474 (2)	5.444 (2)	5.475 (2)	5.454 (2)	5.484 (2)	5.476 (2)
Phase contribution (%)	75	25	55	45	37	63

in the lattice. However, the lattice contraction for the Gd-doped UO_2 gives an opposite effect. It was also reported that the air oxidation product of Gd-doped UO_2 has the composition $(U,Gd)O_{2.4}$, which is even more oxygen-rich than U_3O_7 ($UO_{2.33}$).[15] Tennery and Godfrey[65] obtained O/M = 2.35 for air-oxidized $(U,Pu)O_2$ samples (Pu/(U + Pu) = 0.25). Therefore, it cannot be excluded, even in the current research, that after air oxidation of the La-doped UO_2 samples, the resulting M_4O_9 phase could have excess oxygen beyond the nominal stoichiometry of $MO_{2.25}$.

During low-temperature air oxidation of UO_2, formation of U_4O_9 and U_3O_7 intermediate phases were previously reported by synchrotron X-ray diffraction and neutron diffraction techniques.[66,67] Unfortunately, the analysis of the eventual formation of $U_4O_9/U_3O_7/U_3O_8$ on the surface of the UO_2 sample is not possible with the powder XRD technique, and a surface sensitive technique must be employed (see discussion in the following section).

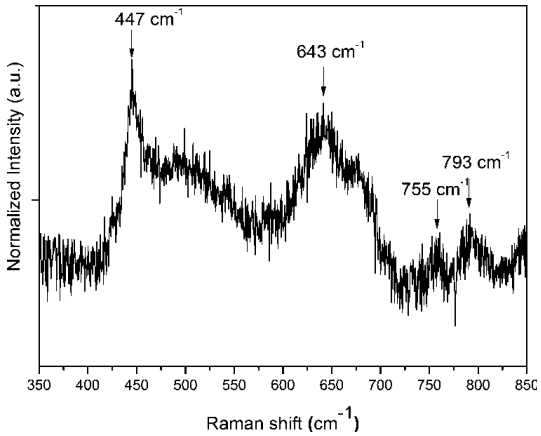

Fig. 10. Raman spectra of air-oxidized UO_2 (conditions: Kr^+ laser at 647 nm, excitation: 2 mW, exposure time:180 s).

(A) Raman Spectroscopy: Raman measurements of the oxidized undoped UO_2 and La-doped UO_2 samples were performed under the same conditions as for non-oxidized samples in order to compare the results. It is known that pure stoichiometric UO_2 in contact with air is readily oxidized, forming an oxidation layer with a depth of approximately 30 nm.[61] A Raman spectrum of the air-oxidized undoped UO_2 sample is shown in Fig. 10. Higher oxides (U_4O_9, U_3O_7, U_3O_8), which were not observed by XRD, are likely precipitating in trace amount on the surface after air oxidation at 500 K for 370 h. Therefore, several bands related to those phases could overlap which could be the reason of lower quality of the Raman Spectra for the oxidized samples and makes difficult to analyze the spectra.

Figure 11 shows the comparison of the normalized Raman spectra of non-oxidized and oxidized La-doped UO_2 samples. It was observed that the principal T_{2g} band gets broadened, shifts to higher wave numbers and significantly decreases in intensity. Moreover, the intensity of the previously observed broad band, which covers the 540 cm^{-1} band (a signature of oxygen vacancies in the structure of La-doped UO_2) and the 570 cm^{-1} LO band, dramatically decreased. Instead, the band at ~630 cm^{-1}, which was attributed to M_4O_9, was clearly observed. These results are therefore in good agreement with the interpretation of Raman results from oxidized La-doped UO_2 samples by different

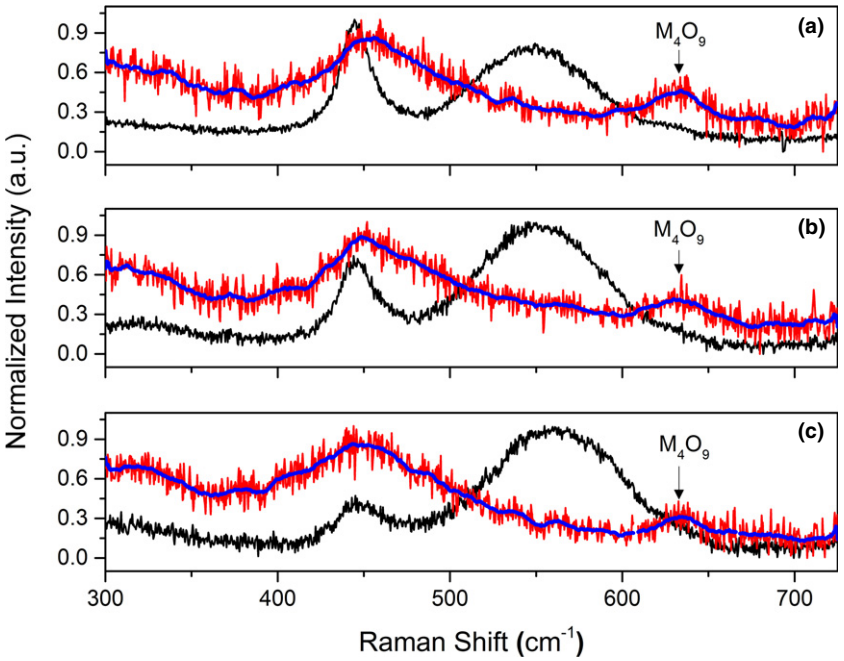

Fig. 11. Comparison of the Raman spectra of the non-oxidized (black line) and air oxidized (blue line (smoothed Raman spectra with the average of 31 points, 630 cm^{-1} peak was shown by arrow) (a) 6 mol% La-doped UO_2, (b) 11 mol% La-doped UO_2, (c) 22 mol% La-doped UO_2 (conditions: Kr^+ laser at 647 nm, excitation: 2 mW, exposure time: 180 s).

laser powers. In addition, the formation of M_4O_9 phase for the oxidized samples was shown both with XRD and Raman Techniques.

In summary, the current research confirms that La-doped uranium dioxide (hypostoichiometric in oxygen) is highly sensitive to oxidation in air. However, oxidation of La-doped UO_2 samples in air at 500 K for 370 h stops with the formation of a M_4O_9 phase.

IV. Conclusions

In this study, UO_2 samples doped with La content varying between 6, 11 and 22 mol% were analyzed using powder XRD and Raman spectroscopy techniques. A single-phase fluorite structure was observed for all the samples.

According to our knowledge, the Raman spectra of uranium–lanthanum-mixed oxides have been reported for the first time with this study. The existence of oxygen vacancies in UO_2 with 6, 11, 22 mol% lanthanum was demonstrated by the presence of a band in the Raman spectra at ~540 cm^{-1}. Raman spectra taken by a 488 nm Ar^+ laser showed oxidation of both pure and La-doped UO_2 samples under the laser, and the inhibition of the formation of M_3O_8 was observed with increasing La content.

The second part of this study describes the low-temperature air oxidation of both UO_2 and La-doped UO_2 samples at 500 K for 370 h. The stabilization of a M_4O_9 structure in the oxidized La-doped UO_2 samples was clearly shown by XRD and Raman spectroscopy. Moreover, the $(U_{1-y}La_y)_4O_9$ phase contribution in oxidized samples increased by increasing La content of the samples. Although XRD results did not show any big difference before and after oxidation for pure UO_2 samples, U_3O_8 formation on the surface was detected by Raman spectroscopy. Under the present oxidation conditions (500 K, 370 h under air), this experimental observation soundly confirms that in La-doped uranium dioxide the prompt air oxidation process stops with the formation of a M_4O_9 phase.

The knowledge of the oxidation behavior of M^{3+}-doped UO_2 samples is important in the context of nuclear technology. As the spent fuel is a complex material, separate effect studies have a great value. La is one of the fission products and therefore these results are important to improve the understanding of the spent fuel oxidation behaviors.

Acknowledgments

We gratefully thank H. Hein and C. Boshoven for the preparation of the La-doped UO_2 samples and D. Bouexiere for XRD measurements and J.- Y. Colle for the measurement of power output from the laser. Z. Talip also gratefully acknowledges the European Commission, Joint Research Centre for funding her grantholder contract.

References

[1]D. C. Hill, "Phase Relations and Crystal Chemistry in the System Uranium Oxide–Lanthanum Oxide," *J. Am. Ceram. Soc.*, **45** [6] 258–63 (1962).

[2]K. Hagemark and M. Broli, "Equilibrium Oxygen Pressures Over Solid Solutions of Urania-Yttria and Urania-Lanthana at 1100°C to 1400°C," *J. Am. Ceram. Soc.*, **50**, 563–7 (1967).

[3]H. G. Diehl and C. Keller, "Das System UO_2-UO_3-$LaO_{1.5}$," *J. Solid State Chem.*, **3**, 621–36 (1971).

[4]E. Stadlbauer, U. Wichmann, U. Lott, and C. Keller, "Thermodynamics and Phase Relationships of the Ternary Lanthanum-Uranium-Oxygen System," *J. Solid State Chem.*, **10**, 341–50 (1974).

[5]T. Matsui and K. Naito, "Electrical Conductivity Measurement and Thermogravimetric Study of Lanthanum-Doped Uranium Dioxide," *J. Nucl. Mater.*, **138**, 19–26 (1986).

[6]T. Fujino, "Thermodynamics of Fluorite Type Solid Solutions Containing Plutonium, Lanthanide Elements or Alkaline Earth Metals in Uranium Dioxide Host Lattices," *J. Nucl. Mater.*, **54**, 14–24 (1988).

[7]H. Kleykamp, "The Solubility of Selected Fission Products in UO_2, and (U, Pu)O_2," *J. Nucl. Mater.*, **206**, 82–6 (1993).

[8]R. V. Krishnan, G. Panneerselvam, M. P. Antony, and K. Nagarajan, "Solubility Studies and Thermal Expansion Coefficient of Uranium–Lanthanum Mixed Oxide System," *J. Nucl. Mater.*, **403**, 25–31 (2010).

[9]K. Yoshida, T. Arima, Y. Inagaki, K. Idemitsu, M. Osaka, and S. Miwa, "Oxygen Potential of Hypo-Stoichiometric La-Doped UO_2," *J. Nucl. Mater.*, **418**, 22–6 (2011).

[10]W. B. Wilson, C. A. Alexander, and A. F. Gerds, "Stabilization of UO_2," *J. Inorg. Nucl. Chem.*, **20**, 242–51 (1961).

[11]H. Landspersky and M. Voboril, "Oxidation of UO_2 Containing Small Additions of Other Oxides," *J. Inorg. Nucl. Chem.*, **29**, 250–2 (1967).

[12]C. R. A. Catlow, "Oxidation Reactions and Dopants in Non-Stoichiometric UO_2," *J. Nucl. Mater.*, **79**, 432–4 (1979).

[13]J.-W. Choi, R. J. McEachern, P. Taylor, and D. D. Wood, "The Effect of Fission Products on the Rate of U_3O_8 Formation in SIMFUEL Oxidized in Air at 250°C," *J. Nucl. Mater.*, **230**, 250–8 (1996).

[14]R. J. McEachern, D. C. Doern, and D. D. Wood, "The Effect of Rare-Earth Fission Products on the Rate of U_3O_8 Formation on UO_2," *J. Nucl. Mater.*, **252**, 145–9 (1998).

[15]L. E. Thomas, R. E. Einziger, and H. C. Buchanan, "Effect of Fission Products on, Air-Oxidation of LWR Spent Fuel," *J. Nucl. Mater.*, **201**, 310–9 (1993).

[16]A. Fernandez, *9th Cimtec, Innovative Materials in Advanced Energy Technologies Part C*. pp. 539. in *proceedings of 9th Cimtec-World forum on new materials*, Syposium VII, Florence, 1999.

[17]Z. Talip, T. Wiss, A. Janssen, J.-Y. Colle, J. Somers, and R. J. M. Konings, "The Dissolution of Helium in La-Doped UO_2 as a Surrogate of Hypostoichiometric UO_2," *Nucl. Mater. Energy* (2015). in press.

[18]J. W. McMurray, D. Shin, and T. M. Besmann, "Thermodynamic Assessment of the U-La-O System," *J. Nucl. Mater.*, **456**, 142–50 (2015).

[19]L. Desgranges, G. Baldinozzi, D. Siméone, and H. E. Fischer, "Refinement of the α-U_4O_9 Crystalline Structure: New Insight into the U_4O_9-U_3O_8 Transformation," *Inorg. Chem.*, **50**, 6146–51 (2011).

[20]http://www.ill.eu/sites/fullprof/ (accessed on 04 March 2015).

[21]J. Rodriguez-Carvajal, "Recent Advances in Magnetic Structure Determination by Neutron Powder Diffraction," *Phys. B*, **192**, 55–69 (1993).

[22]T. Roisnel and J. Rodriguez-Carvajal, "WinPLOTR: A Windows Tool for Powder Diffraction Patterns," *Materials Science Forum*, **378-381**, 118–23 (2000).

[23]J. H. Parker Jr., D. W. Feldman, and M. Ashkin, "Raman Scattering by Silicon and Germanium," *Phys. Rev.*, **155**, 712–4 (1967).

[24]K. H. Desai, R. W. Grimes, D. Parfitt, T. Wiss, and P. Van Uffelen, "Atomic-Scale Simulation of Soluble Fission Products in UO_2"; EUR Report ISSN 1018-5593, 2009.

[25]D. Shin and T. M. Besmann, "Thermodynamic Modelling of the (U,La) $O_{2\pm x}$ Solid Phase," *J. Nucl. Mater.*, **433**, 227–32 (2013).

[26]T. Ohmichi, S. Fukushima, A. Maeda, and H. Watanabe, "On the Relation Between Lattice Parameter and O/M Ratio for Uranium Dioxide-Trivalent Rare Earth Oxide Solution," *J. Nucl. Mater.*, **102**, 40–6 (1981).

[27]R. V. Krishnan, V. K. Mittalb, R. Babua, A. Senapatia, S. Berab, and K. Nagarajana, "Heat Capacity Measurements and XPS Studies on Uranium–Lanthanum Mixed Oxides," *J. Alloy. Compd.*, **509**, 3229–37 (2011).

[28]J. Hertog, "Lattice Parameter Evolution of Single Doped and Co-Doped UO_2 Systems"; External Report of the Belgian Nuclear Research Centre SCK CEN-ER-175, June, 2011.

[29]T. Tsuji, M. Iwashita, T. Yamashita, and K. Ohuchi, "Effect of Cations on Lattice Constants of $(M_yU_{1-y})O_{2.00}$ (M=Pu, Th, La) at Low Doped Cation Concentrations," *J. Alloy. Compd.*, **271–273**, 391–4 (1998).

[30]C. Gueneau, A. Chartier, and L. Van Brutzel, "Thermodynamic and Thermophysical Properties of the Actinide Oxides," *Comp. Nucl. Matter*, **2**, 21–59 (2012).

[31]P. R. Graves, "Raman Microprobe Spectroscopy of Uranium Dioxide Single Crystal and Ion Implanted Polycrystals," *Appl. Spectrosc.*, **44**, 1665–7 (1990).

[32]G. M. Begun, R. G. Haire, W. R. Wilmarth, and J. R. Peterson, "Raman Spectra of Some Actinide Dioxides and of EuF_2," *J. Less Common Metals*, **162**, 129–33 (1990).

[33]P. G. Marlow, J. P. Russell, and J. R. Hardy, "Raman Scattering in Uranium Dioxide," *Philos. Mug.*, **14**, 409–10 (1966).

[34]G. C. Allen, I. S. Butler, and N. A. Tuan, "Characterization of Uranium of Uranium Oxides by Micro-Raman Spectroscopy," *J. Nucl. Mater.*, **144**, 17–9 (1987).

[35]M. Amme, B. Renker, B. Schmid, M. P. Feth, H. Bertagnolli, and W. Dobelin, "Raman Microspectrometric Identification of Corrosion Products Formed on UO_2 Nuclear Fuel During Leaching Experiments," *J. Nucl. Mater.*, **306**, 202–12 (2002).

[36]H. Idriss, "Surface Reactions of Uranium Oxide Powder, Thin Films and Single Crystals," *Surf. Sci. Rep.*, **65**, 67–109 (2010).

[37]T. Livneh and E. Sterer, "Effect of Pressure on the Resonant Multiphonon Raman Scattering in UO_2," *Phys. Rev. B*, **73**, 085118, 9pp (2006).

[38]D. Manara and B. Renker, "Raman Spectra of Stoichiometric and Hyperstoichiometric Uranium Dioxide," *J. Nucl. Mater.*, **321**, 233–7 (2003).

[39]L. Desgranges, G. Baldinozzi, P. Simon, G. Guimbretiere, and A. Canizares, "Raman Spectrum of U_4O_9: A New Interpretation of Damage Lines in UO_2," *J. Raman Spectrosc.*, **43**, 455–8 (2012).

[40]H. He, M. Broczkowski, K. O'Neil, D. Ofori, O. Semenikhin, and D. Shoesmith, "Corrosion of Nuclear Fuel (UO_2) Inside a Failed Nuclear Waste Container"; NWMO TR-2012-09, Western University, Ontario, Canada, 2012.

[41]H. He, Z. Ding, and D. W. Shoesmith, "The Determination of Electrochemical Reactivity and Sustainability on Individual Hyper-Stoichiometric UO_{2+x} Grains by Raman Microspectroscopy and Scanning Electrochemical Microscopy," *Electrochem. Commun.*, **11**, 1724–7 (2009).

[42]H. He and D. Shoesmith, "Raman Spectroscopic Studies of Defect Structures and Phase Transition in Hyper-Stoichiometric UO_{2+x}," *Phys. Chem. Chem. Phys.*, **12**, 8108–17 (2010).
[43]M. J. Sarsfield, R. J. Taylor, C. Puxley, and H. M. Steele, "Raman Spectroscopy of Plutonium Dioxide and Related Materials," *J. Nucl. Mater.*, **427**, 333–42 (2012).
[44]T. Taniguchi, T. Watanabe, N. Sugiyama, A. K. Subramani, H. Wagata, N. Matsushita, and M. Yoshimura, "Identifying Defects in Ceria-Based Nanocrystals by UV Resonance Raman Spectroscopy," *J. Phys. Chem. C*, **113**, 19789–93 (2009).
[45]M. Razdan and D. W. Shoesmith, "Influence of Trivalent-Dopants on the Structural and Electrochemical Properties of Uranium Dioxide (UO_2)," *J. Electrochem. Soc.*, **161**, 105–13 (2014).
[46]J. R. McBride, K. C. Hass, B. D. Poindexter, and W. H. Weber, "Raman and X-ray Studies of $Ce_{1-x}REO_{2-y}$, Where RE=La, Pr, Nd, EU, Gd and Tb," *J. App. Phys.*, **76**, 2435–41 (1994).
[47]Z.-Y. Pu, J.-Q. Lu, M.-F. Luo, and Y.-L. Xie, "Study of Oxygen Vacancies in $Ce_{0.9}Pr_{0.1}O_{2-\delta}$ Solid Solution by *In Situ* X-ray Diffraction and *In Situ* Raman Spectroscopy," *J. Phys. Chem.*, **111**, 18695–702 (2007).
[48]L. Li, F. Chen, J.-Q. Lu, and M.-F. Luo, "Study of Defect Sites in $Ce_{1-x}M_xO_{2-\delta}$ (x = 0.2) Solid Solutions Using Raman Spectroscopy," *J. Phy. Chem*, **115**, 7972–7 (2011).
[49]A. Oaks, D. Yun, B. Ye, W.-Y. Chen, and J. F. Stubbins, "Kinetic Monte Carlo Model of Defect Transport and Irradiation Effects in La-Doped CeO_2," *J. Nucl. Mater.*, **414**, 145–9 (2011).
[50]D. Yun, A. J. Oaks, W. Chen, M. A. Kirk, J. Rest, Z. Z. Insopov, A. M. Yacout, and J. F. Stubbins, "Kr and Xe Irradiations in Lanthanum (La) Doped Ceria: Study at the High Dose Regime," *J. Nucl. Mater.*, **418**, 80–6 (2011).
[51]B. Ye, D. Yun, A. J. Oaks, W. Chen, M. A. Kirk, J. Rest, A. M. Yacout, and J. F. Stubbins Yun, "The Effects of Xenon Implantation in Ceria with and Without Lanthanum," *Nucl. Instrum. Methods Phys. Res., Sect. B*, **272**, 236–8 (2012).
[52]D. Yun, B. Yeb, A. J. Oaks, W. Chen, M. A. Kirk, J. Rest, A. M. Yacout, and J. F. Stubbins, "Fission Gas Transport and Its Interactions with Irradiation-Induced Defects in Lanthanum Doped Ceria," *Nucl. Instrum. Methods Phys. Res., Sect. B*, **272**, 239–43 (2012).
[53]G. Guimbretiére, L. Desgranges, A. Canizares, G. Carlot, R. Caraballo, C. Jégou, F. Duval, N. Raimboux, M. R. Ammar, and P. Simon, "Determination of In-Depth Damaged Profile by Raman Line Scan in Pre-cut He^{2+} Irradiated UO_2," *Appl. Phys. Lett.*, **100**, 251914, 4pp (2012).
[54]L. Desgranges, G. Guimbretière, P. Simon, F. Duval, A. Canizares, R. Omnee, C. Jegou, and R. Caraballo, "Annealing of the Defects Observed by Raman Spectroscopy in UO_2 Irradiated by 25 MeV He^{2+} Ions," *Nucl. Instrum. Methods Phys. Res., Sect. B*, **327**, 74–7 (2014).
[55]L. Desgranges, G. Guimbretière, P. Simon, C. Jegou, and R. Caraballo, "A Possible New Mechanism for Defect Formation in Irradiated UO_2," *Nucl. Instrum. Methods Phys. Res., Sect. B*, **315**, 169–72 (2013).
[56]L. Desgranges, Y. Pontillon, P. Matheron, M. Marcet, P. Simon, G. Guimbretiére, and F. Porcher, "Miscibility Gap in the U–Nd–O Phase Diagram: A New Approach of Nuclear Oxides in the Environment?" *Inorg. Chem.*, **51**, 9147–9 (2012).
[57]R. Rao, R. K. Bhagat, N. P. Salke, and A. Kumar, "Raman Spectroscopic Investigation of Thorium Dioxide-Uranium Dioxide (ThO_2-UO_2) Fuel Materials," *Appl. Spectrosc.*, **68**, 44–8 (2014).
[58]M. L. Palacios and S. H. Taylor, "Characterization of Uranium Oxides Using *In Situ* Micro-Raman Spectroscopy," *Appl. Spectrosc.*, **54**, 1372–8 (2000).
[59]C. Jégou, R. Caraballo, S. Peuget, D. Roudil, L. Desgranges, and M. Magnin, "Raman Spectroscopy Characterization of Actinide Oxides ($U_{1-y}Pu_y$) O_2: Resistance to Oxidation by the Laser Beam and Examination of Defects," *J. Nucl. Mater.*, **405**, 235–43 (2010).
[60]I. S. Butler, G. C. Allen, and N. A. Tuan, "Micro Raman Spectrum of Triuranium Octoxide, U_3O_8," *App. Spect*, **42**, 901–2 (1988).
[61]R. J. McEachern and P. Taylor, "A Review of the Oxidation of Uranium Dioxide at Temperatures Below 400°C," *J. Nucl. Mater.*, **254**, 87–121 (1998).
[62]K. Kim and D. Olander, "Oxygen Diffusion in UO_{2-x}," *J. Nucl. Mater.*, **102**, 192–9 (1981).
[63]Y. K. Ha, J. G. Kim, Y. J. Park, and W. H. Kim, "Effect of Tetravalent Dopant, Th^{4+} on the Oxidation of Uranium Dioxide," *Key Eng. Mater.*, **277–279**, 654–9 (2005).
[64]J. G. Kim, Y. K. Ha, S. D. Park, K. Y. Lee, and W. H. Kim, "Effect of a Trivalent Dopant, Gd^{3+}, on the Oxidation of Uranium Dioxide," *J. Nucl. Mater.*, **297**, 327–31 (2001).
[65]V. J. Tennery and T. G. Godfrey, "Oxidation Properties of (U,Pu)O_2 Solid Solutions," *J. Am. Chem. Soc.*, **56**, 129–33 (1973).
[66]G. Rousseau, L. Desgranges, J.-C. Niépce, J.-F. Bérar, and G. Baldinozzi, "Contribution of the Synchrotron Diffraction Study of the Oxidation of Uranium Dioxide at 250°C," *J. Phys. IV Fr*, **118**, 127–34 (2004).
[67]L. Desgranges, G. Baldinozzi, G. Rousseau, J.-C. Niépce, and G. Calvarin, "Neutron Diffraction Study of the *In Situ* Oxidation of UO_2," *Inorg. Chem.*, **48**, 7585–92 (2009). □